



ORIGINAL ARTICLE

Influence of polycrystalline MoS₂ nanoflowers on mouse breast cancer cell proliferation *via* molten salt sintering



Xue Wang^{a,1}, Mengli Zhao^{b,1}, Jianmin Feng^a, Dejun Li^{a,*}

^a College of Physics and Materials Science, Tianjin Normal University, Tianjin 300387, China

^b School of Electronic Engineering, Chaohu University, Anhui 238024, China

Received 22 July 2022; accepted 13 January 2023

Available online 20 January 2023

KEYWORDS

Molybdenum disulfide;
Molten salt sintering;
Nanoflowers;
Mouse breast cancer cells;
Proliferation

Abstract In this paper, polycrystalline molybdenum disulfide (MoS₂) nanoflowers were prepared by mixing ammonium molybdate tetrahydrate [(NH₄)₆Mo₇O₂₄·4H₂O] and potassium thiocyanate (KSCN) at 300 °C for 2 h *via* molten salt sintering method. Under scanning electron microscope (SEM) and high-resolution transmission electron microscope (HRTEM), MoS₂ showed popcorn-like shape, which surface distribution defects were easy to be further modified. MoS₂ as a nano-enzyme was used to inhibit the proliferation of mouse breast cancer cells (4 T1), which had 69.8 % inhibitory effect on 4 T1 cell proliferation. Electron spin resonance (ESR) analysis showed that MoS₂ could produce a large number of stable hydroxyl radicals (–OH). The disulfide bond in MoS₂ was highly sensitive to reactive oxygen species (ROS). High ROS level leads to the death of cancer cells under oxidative stress and inhibits the proliferation of 4 T1. This work demonstrates that MoS₂ is a potential anticancer drug or carrier for cancer treatment.

© 2023 The Authors. Published by Elsevier B.V. on behalf of King Saud University. This is an open access article under the CC BY-NC-ND license (<http://creativecommons.org/licenses/by-nc-nd/4.0/>).

1. Introduction

As a disease with high mortality, the treatment of cancer has always been an important research direction (Jaya Seema et al., 2018; Saifullah et al., 2018; Bullo et al., 2019; Mousavi et al., 2019; Liu et al., 2013; Abbas et al., 2015). For a long time, the efficacy of traditional anticancer drugs and chemotherapy has been low, because in the process of cancer treatment, it will inevitably produce toxicity to human normal tissues and bring serious toxic and side effects to cancer patients (Curigliano et al., 2016). Patients need new medical treatments to resist the damage of malignant tumor cells.

Human beings need new drugs. The rapid development of nanotechnology provides us with a new direction. The research and development of nanotherapeutic drugs to treat tumor diseases are urgent (Murugesan et al., 2018; Kundu et al., 2019). In recent years, the pro-

* Corresponding author at: College of Physics and Materials Science, Tianjin Normal University, Tianjin 300387, China.

E-mail addresses: zml0506@tjnu.edu.cn (M. Zhao), dejunli@tjnu.edu.cn (D. Li).

¹ These authors contributed equally to this work.

Peer review under responsibility of King Saud University.



posal and development of nano catalytic medicine (NCM) have brought potential treatment schemes for cancer. Nontoxic or slightly toxic nanoparticles (NPS) are introduced into pathological areas as nano catalytic reactants to start the tumor treatment mechanism, to achieve the purpose of sustainable treatment and more biocompatibility through “catalytic” therapeutic chemical reaction. NCM has high specificity in reducing side effects. Different from the traditional delivery model of therapeutic agents, the inherent substances in the pathogenic environment are used for catalytic treatment (Yang et al., 2019). In NCM, chemokinetic therapy (CDT) is a cancer treatment mode that is activated by chemical stimulation and produces ROS (Zhang et al., 2016). Based on the characteristic pathological and chemical characteristics of tumor microenvironment (TME), mild acidity and excessive H_2O_2 are conducive to the catalytic reaction in the tumor, resulting in the production of a large number of toxic $-OH$, the increase of ROS level, oxidative stress reaction in the tumor, cancer cell death and tissue damage. It has been used to provide nano catalytic therapy to deal with malignant tumors and reduce toxicity *in vivo* (Wang et al., 2018; Hanahan and Weinberg, 2011).

With the continuous development and expansion of the field of NCM, as a new branch of nanomedicine, it still has challenges such as low biodegradability and few catalytic active sites after surface modification, which requires the coordination of catalytic activity and surface modification to alleviate the challenges (Yang et al., 2019; Arami et al., 2015; Mout et al., 2012). Individual nano-catalyst needs to be functionally modified on the surface of nanocarriers that can improve reaction activity (Yang et al., 2019). For example, MoS_2 nano sheets doped with copper ions can effectively kill bacteria under light (Wang et al., 2020). MoS_2 /ferrous sulfide (FeS) heterojunction and rhein (Rhe) anti-inflammatory drugs form microwave responsive MoS_2 /FeS/Rhe to help kill bacteria and effectively eradicate rat tibial osteomyelitis infected by *Staphylococcus aureus* (Jin et al., 2022). Ag/ MoS_2 showed high level ROS killing bacteria and strong photocatalytic activity (Zhu et al., 2020). The photodynamic and photothermal properties of chitosan combined with MoS_2 (CS@ MoS_2) showed excellent surface self-antibacterial ability (Feng et al., 2018). Two dimensional (2D) MoS_2 has a unique high specific surface area, adjustable band gap, high efficiency near infrared photothermal conversion and good biocompatibility, which can be used for antibacterial research by photothermal or photodynamic (Chen et al., 2022). Hydrothermal synthesis of CuS/graphene oxide (GO) hybrid. High specific surface area CuS/GO and a large number of defects in GO improve the photocatalytic properties of the hybrid, showing excellent antibacterial effect and good biocompatibility (Lv et al., 2022). The representative new 2D nanomaterials (2DNMs), such as transition metal glycols, have great application prospects in the antibacterial field due to their adjustable band gap, crystal structure characteristics, migration carriers and restrictions on thermal diffusion (Li et al., 2022). In order to maximize the effect of catalytic therapy, it may be a feasible and effective method to combine different material components to make them work together. (Xing et al., 2018). Have shown that metal sulfides (MoS_2 , ZnS, Cr_2S_3 , CoS_2 , PbS, or WS_2) are used as cocatalysts to improve catalytic efficiency, and enhance Fenton reaction efficiency by exposing metal active sites and proton capture (Li et al., 2016; Ran et al., 2017). Typical transition metal dihalide compounds (TMDs) 2DNMs MoS_2 and its nanocomposites show great potential in the field of cancer treatment due to their excellent antibacterial and anticancer activities (Zhou et al., 2021; Jiang et al., 2021; Tan et al., 2016; Zhang et al., 2020; Yang et al., 2020). It has attracted extensive attention in the field of nano medicine. The 2D MoS_2 belongs to the hexagonal system, which is formed by stacking metal molybdenum (Mo) atoms between sulfur (S) atomic layers. There is a covalent bond between Mo and S. The Van der Waals force stacking structure is similar to the MoS_2 sheets of graphite layer, and the layer spacing of MoS_2 is larger than that of graphite, which provides a large network for surface functional modification (Liu et al., 2022; Chong et al., 2021; Gao et al., 2018; Wu et al., 2019; Kasinathan et al., 2021; He et al., 2020). In addition, unlike most inorganic nanomaterials, MoS_2 can be discharged from the kidney

within one month due to its excellent biocompatibility, avoiding the toxic harm of long-term retention to organisms (Zhang et al., 2018). With the continuous development of tumor treatment research on MoS_2 and its nanocomposites, there are few studies on excellent nano catalytic carriers. In order to carry out surface functional modification engineering on its substrate and play a greater anti-cancer effect, we need a kind of auxiliary nano catalytic carrier, which has a strong CDT therapeutic effect when it acts alone.

Therefore, the polycrystalline MoS_2 with spherical nanowire structure was prepared by the low-temperature molten salt method, and its anticancer effect was studied using 4 T1. We also analyzed the anticancer mechanism of MoS_2 by SEM, HRTEM, X-ray photoelectron spectroscopy (XPS), ESR, and laser confocal microscope. MoS_2 can produce stable $-OH$, triggering oxidative stress reaction of tumor cells at high ROS level, resulting in cell hypoxia death. It can effectively inhibit the proliferation of cancer cells.

2. Material and methods

2.1. Cell culture

Mouse fibroblasts (L929) and 4 T1 were purchased by Tianjin Jinze New Technology Co., Ltd. (Tianjin, China). L929 in DMEM (Gibco, USA) medium containing 1 % penicillin Streptomycin Solution (HyClone, Utah) and 10 % Foetal Bovine Serum (FBS, Gibco, Australia) at 37 °C and 5 % CO_2 constant temperature incubator. 4 T1 were cultured in 89 % RPMI-1640 (BIOIND, Israel) medium with 1 % penicillin–streptomycin solution and 10 % FBS at 37 °C and 5 % CO_2 constant temperature incubator.

2.2. Preparation of molybdenum disulfide by molten salt sintering

5 g KSCN (99 %, 3A) and 0.15 g $(NH_4)_6Mo_7O_{24} \cdot 4H_2O$ (99 %, Aladdin) were evenly mixed and put into a muffle furnace (LFM1200C box furnace, Hefei Compain Equipment Technology Co., Ltd.), heated to 300 °C for 2 h to prepare MoS_2 . After the reaction, dissolve the black solid with deionized water to filter and wash off the excess KSCN, and then dried in a vacuum oven (DZF-6050 vacuum oven, Hefei Kejing Material Technology Co., Ltd.) at 80 °C for 24 h. Fig. 1 shows the manufacturing process of MoS_2 .

2.3. Material characterization

The surface morphology of MoS_2 was observed by SEM (SU-8010, Hitachi, Japan). The nano-sized high-resolution structural characteristics and composition of the samples were studied by HRTEM (Talos F200x, Thermo Fisher Scientific, Czech Republic) combined with high-resolution lattice fringe image, selected area electron diffraction (SAED), and energy dispersive spectroscopy (EDS) element mapping. XPS (PHI5000 VersaProbe, ULVAC-PHI, Japan) was used to analyze the composition of surface elements, the chemical state, and molecular structure of surface elements. And the contaminated carbon (284.8 eV) was used for energy correction.

2.4. Enzyme activity and hydroxyl radical recognition

The peroxidase (POD)-like catalytic activity of MoS_2 nano enzyme was analyzed *via* 3,3',5,5'-tetramethylbenzene (TMB,

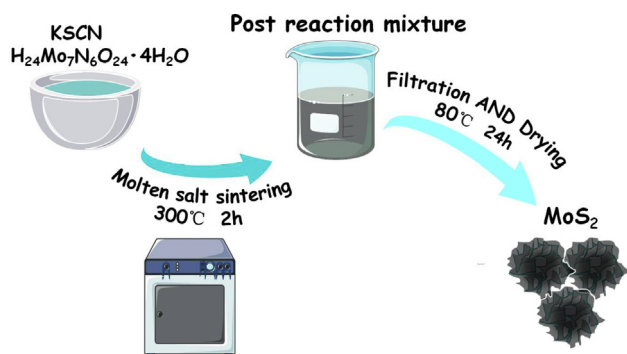


Fig. 1 Sample preparation process.

Solarbio) colorless POD substrate. The formation of blue oxidized TMB (oxTMB) was detected in acidic HAc-NaAc buffer (0.2 M, pH = 3.6) using the ultraviolet visible spectrometer (UV-3600, SHIMADZU, Japan). Meanwhile, H₂O₂ with different concentrations (0, 5, 10 and 20 mM) were respectively added into the mixed system of 1.8 mL HAc-NaAc buffer (0.2 M, pH = 3.6), 0.1 mL TMB solution and 0.1 mL MoS₂ (50 µg/mL) reaction at 37 °C. After the reaction, the change curve of absorbance with reaction time was measured at 652 nm with ultraviolet visible spectrometer. ESR analysis experiment was used for free radical identification, which was carried out by electron spin resonance spectrometer (EMXplus-6/1, Bruker, Germany). 11 µL of the spin-trap 5,5-dimethyl-1-pyrroline *N*-oxide (DMPO, 500 mM, Shanghai McLean Biochemical Technology Co., Ltd., China) was added into 70 µL MoS₂ (1 mg/mL) and 49 µL phosphate buffer (PBS, 0.01 M, pH = 6.5, Shanghai Yuanye Biotechnology Co., Ltd., China) with and without 70 µL H₂O₂ (300 µM). The reaction system was sucked into the capillary tube and sealed with silicone grease. After the capillary tube was wiped clean, it was put into a paramagnetic tube. The formation of -OH was verified at room temperature with microwave operating frequency of 9.8 GHz in the X-band.

2.5. *In vitro* cytocompatibility and cytotoxicity analysis

A logarithmic long-term L929 or 4 T1 was inoculated with 1 mL cell suspension (planting density of 1×10^4 cell/mL) on 24 well plates. After incubating for 24 h in a constant temperature incubator at 37 °C, a vacuum pump was used to suck out the culture medium. MoS₂ was diluted to different concentrations (12.5 µg/mL, 25 µg/mL, 50 µg/mL, 100 µg/mL, 200 µg/mL) and added to each experimental hole by culture medium, and incubated at 37 °C incubator for different times (2 h, 6 h, 12 h, 24 h). Suck the supernatant and add 300 µL of serum free media containing 10 µL Cell Counting Kit-8 (CCK-8, Genview) into each well. After incubation in the incubator for 2 h, transfer 300 µL of CCK-8 mixture to 3 wells of 96 well plate, 100 µL per well. It is defined that the hole survival rate of blank medium per well is 0 %, and the hole survival rate of complete medium and cells is 100 %. The optical density (OD) of three experimental holes in each group was recorded by an enzyme-labeled instrument (ELX808IU, BioTek, USA) at the wavelength of 450 nm.

2.6. Observation of living and dead cells by laser confocal microscope

Calcein-AM and PI (Beyotime) were co-stained with L929 or 4 T1 to detect cell activity and cytotoxicity. Firstly, the L929 or the 4 T1 cell suspension (planting density of 3×10^4 cell/mL) was inoculated on the special confocal culture dish (Biosharp), and cultured in the 37 °C in-cubator for 24 h. Then the supernatant was sucked away and added to MoS₂/culture medium mixture for 12 h. Next sucked out the culture medium and washed the cells with cold PBS. Lastly, 0.3 µL Calcein-AM, 0.3 µL PI, and 3 µL detection buffer were mixed. The mixture was added to the experimental confocal dish with 300 µL per well and was incubated in the dark at 37 °C for 40 min. After incubation, the samples were observed under laser confocal microscope (FV1000, Olympus, Japan). Calcein-AM showed green fluorescence (Ex/Em = 488/517 nm) and PI showed red fluorescence (Ex/Em = 546/617 nm).

2.7. Statistical analysis

Data were expressed as mean ± Standard error of mean (SEM) and were evaluated using one-way ANOVA followed by Tukey's multiple comparisons test (GraphPad Prism version 9.0; GraphPad Software, La Jolla, CA, USA) to determine statistically significant differences. **P* < 0.05 was represented statistically significant.

3. Results and discussion

3.1. Surface structure analysis

The morphology of MoS₂ was characterized by SEM, as shown in Fig. 2a and b. MoS₂ is spherical, and its surface is wrapped by layered gullies. The spherical stacking of popcorn makes its surface area large. Fig. 2c-e shows the HAADF-STEM image and EDS element mapping images of MoS₂, which proves the successful synthesis of MoS₂. It can be clearly observed that Mo and S are evenly distributed in the structure of MoS₂ nanoflower. As shown in Fig. 2f, the micro surface morphology was further analyzed by TEM, in which the surface was flower pleated and distributed with multi-layer thin nanolayers. Next, combine the HAADF-STEM image and its corresponding Fourier transform (FT), as shown in Fig. 2g. The clear lattice arrangement on the surface of MoS₂ nanoflowers indicates that it has good crystallinity. It is worth noting that there are obvious defects at the surface gullies as shown in the circle in the figure, which can be further modified. The surface lattice spacing is 0.256 nm, corresponding to MoS₂ (102) plane (Zhou et al., 2021). Fourier transform images show that MoS₂ is polycrystalline. SAED image is shown in Fig. 2h, which further verified that MoS₂ is polycrystalline. (101) and (106) planes also exist in MoS₂.

In addition, the elemental composition and molecular structure of MoS₂ were studied by XPS. Fig. 3a shows the full XPS spectrum of MoS₂. It also shows the successful preparation of MoS₂. Fig. 3b shows the Mo 3d spectra with five peaks. The peaks located at 228.6 eV (3d_{5/2}) and 231.7 eV (3d_{3/2}) correspond to Mo-S of 1 T (octahedral) MoS₂ (Fan et al., 2017). In addition, the double peaks are located at 232.5 eV and

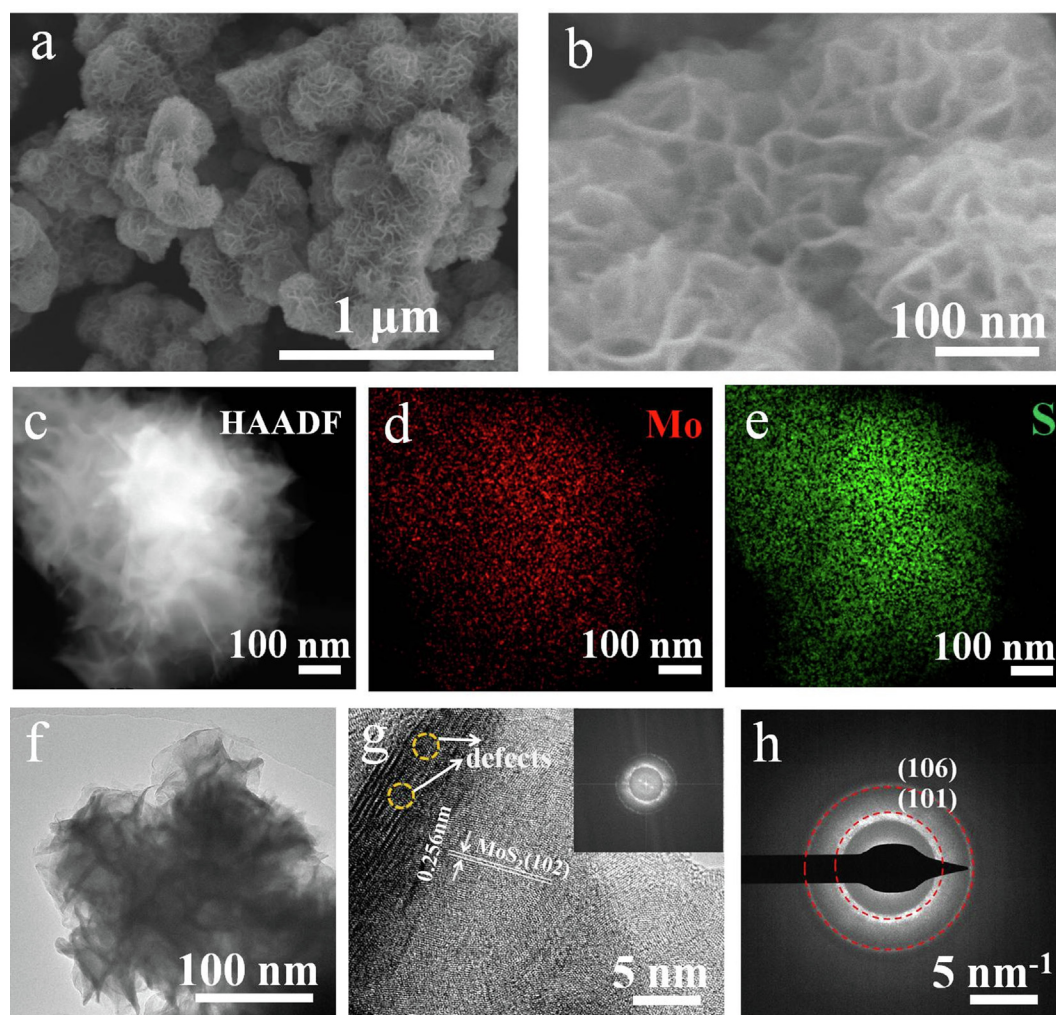


Fig. 2 (a, b) SEM images of MoS₂. (c-e) HAADF-STEM image and EDS element mapping of MoS₂. (f) TEM image of MoS₂. (g) HRTEM morphology of MoS₂ and the corresponding FT patterns (inset). (h) SAED image of MoS₂.

235.6 eV, belonging to Mo-O of 2H (triangular cylindrical) MoS₂ (Li et al., 2016). The peak position of 225.8 eV belongs to S 2s. O 1s spectra in Fig. 3c, the peak position of 531.03 eV belongs to Mo-O. According to the S 2p spectra in Fig. 3d, the peaks observed at 161.5 eV (2p_{3/2}) and 162.7 eV (2p_{1/2}) correspond to Mo-S and belonged to the 1T phase. The bimodal 162.8 eV and 163.9 eV belong to the 2H phase.

The nano enzyme with POD-like activity can induce H₂O₂ to decompose into -OH, and TMB is oxidized by -OH to form blue oxTMB in Fig. 4a (Gao et al., 2007; Gao et al., 2019). Fig. 4b shows that there is no obvious characteristic peak in the absorbance of the reaction system without MoS₂, indicating that there is no oxidation reaction. In the reaction mixture of TMB + H₂O₂ + MoS₂, there are two absorbance characteristic peaks at 370 and 652 nm. It is observed that the solution is obviously blue, which confirms that MoS₂ has inherent nano enzyme POD-like activity. Under the action of H₂O₂ at different concentrations (0, 5, 10 and 20 mM), the time absorbance change curves of the reaction product oxTMB are shown in Fig. 4c. It is found that the absorbance of MoS₂ is the strongest at 20 mM H₂O₂, and a concentration gradient

dependent color curve is presented at different H₂O₂ concentrations. This confirms that MoS₂ and H₂O₂ can generate -OH. ESR analyses of MoS₂ with or without H₂O₂ using DMPO spin-trapping agent are shown in Fig. 4d. In the presence of H₂O₂, the ESR spectra of MoS₂ showed the (1:2:2:1) characteristic signal of -OH with DMPO as the -OH capture agent (Zhang et al., 2020). Because cancer cells contain a large amount of H₂O₂ in the unique TME environment, in the acidic environment, the -OH characteristic signal of the ESR map indicates that MoS₂ has a high level of ROS, leading to intense redox reaction in cancer cells, while the disulfide bond in MoS₂ is highly sensitive to redox and easy to break, which is easy to release effective therapeutic substances (Ranucci et al., 2008; Park et al., 2010; Wu et al., 2015). This means that MoS₂ can cause oxidative stress and hypoxia death of cancer cells.

3.2. Cell proliferation toxicity test

Firstly, the CCK-8 system was used to study the proliferation of L929 cells by MoS₂ at different concentrations, as shown in Fig. 5a. It can be clearly observed that there is no difference in

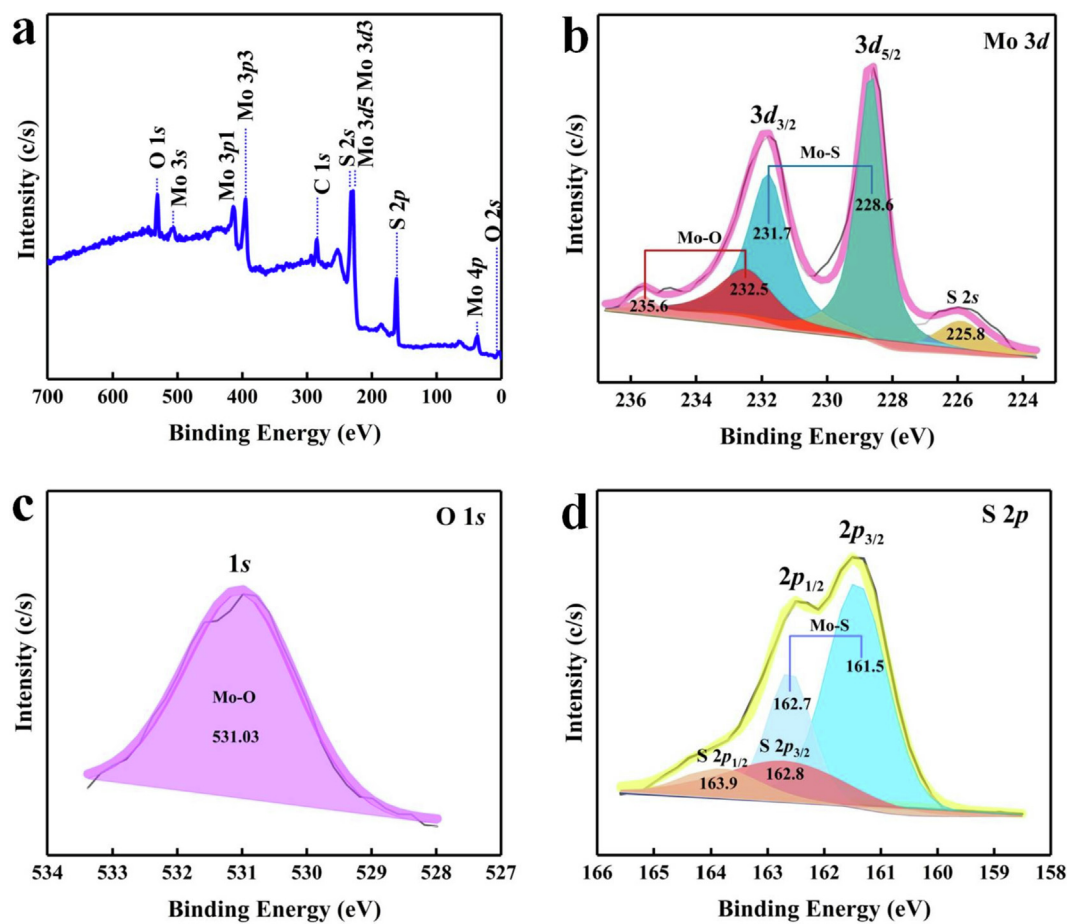


Fig. 3 (a) XPS spectrum of MoS₂, (b) Mo 3d, (c) O 1 s, (d) S 2p.

cell survival between the sample (MoS₂ concentration of 25 $\mu\text{g}/\text{mL}$) and the control group (MoS₂ concentration of 0 $\mu\text{g}/\text{mL}$). The cell survival rate of L929 is 84.9 % at the concentration of 50 $\mu\text{g}/\text{mL}$, and MoS₂ has almost no significant inhibitory effect on L929. When the concentration is increased to 200 $\mu\text{g}/\text{mL}$, the cell survival rate is 72.8 %, and MoS₂ has only slight cytotoxicity to L929. It is proved that there is no significant cytotoxicity at lower concentrations of MoS₂ (≤ 100 $\mu\text{g}/\text{mL}$). Then, the anticancer effect of MoS₂ on 4 T1 *in vitro* was studied by the CCK-8 system, as shown in Fig. 5b and c. It can be clearly seen that the proliferation of 4 T1 cells decrease step by step when MoS₂ and 4 T1 were co-incubated from 2 h to 24 h. With the increase of time, MoS₂ caused the oxidative stress reaction in 4 T1 cells. Toxic -OH induced apoptosis of 4 T1 cells in anoxic environment. After 12 h, MoS₂ has a significant inhibitory effect on the proliferation of 4 T1 as shown in Fig. 5b. Especially for 24 h, the survival rate of 4 T1 cells decreased to only about 30 %. In addition, the results also show that the concentrations of MoS₂ also affect the viabilities of 4 T1 cells. With the increase of MoS₂ concentration, the survival rate of 4 T1 cells decreased, especially for 24 h culture. Therefore, different concentrations of MoS₂ incubated with 4 T1 were also studied as shown in Fig. 5c. When the dose of MoS₂ is 12.5 $\mu\text{g}/\text{mL}$, the cell survival rate of 4 T1 is 56.7 %, indicating that a small dose of MoS₂ may significantly inhibit the proliferation of 4 T1 cells. When the concentration

increases to 200 $\mu\text{g}/\text{mL}$, the cell survival rate is only 30.2 %. The antitumor effect of MoS₂ with 200 $\mu\text{g}/\text{mL}$ is the most obvious of all the samples, which indicates that the MoS₂ nanoparticles are swallowed by cells, more cell death. Inhibition of 4 T1 cell proliferation is positively correlated with the concentration and action time of MoS₂. The results indicate that the almost negligible cytotoxicity of MoS₂ against L929 brought about good cytocompatibility, with little effect compared to the strong inhibition against tumor cells. The cytotoxicity of MoS₂ against tumor cells is attributed to the catalytic therapeutic response under the TME. MoS₂ triggers massive toxic -OH induced killing of 4 T1 tumor cells.

Confocal images of L929 fluorescence in Fig. 6 show that after Calcein-Am and PI was co-stained, the MoS₂ treated group embodied good cell viability indistinguishable from the control group, and L929 exhibited good cell morphology with intact cell membranes and no dead cells, indicating the same results as the cytotoxicity assay. The fluorescence confocal images of 4 T1 treated by the control group and MoS₂ were used to further verify the effectiveness of CCK-8. 4 T1 was co-stained with Calcein-Am and PI, as shown in Fig. 6. The results are divided into two groups. Which are cell survival and cell death. There was no significant change in 4 T1 in the control group and 4 T1 cells proliferated and adhered well. On the contrary, 4 T1 in the MoS₂ treatment group resulted in

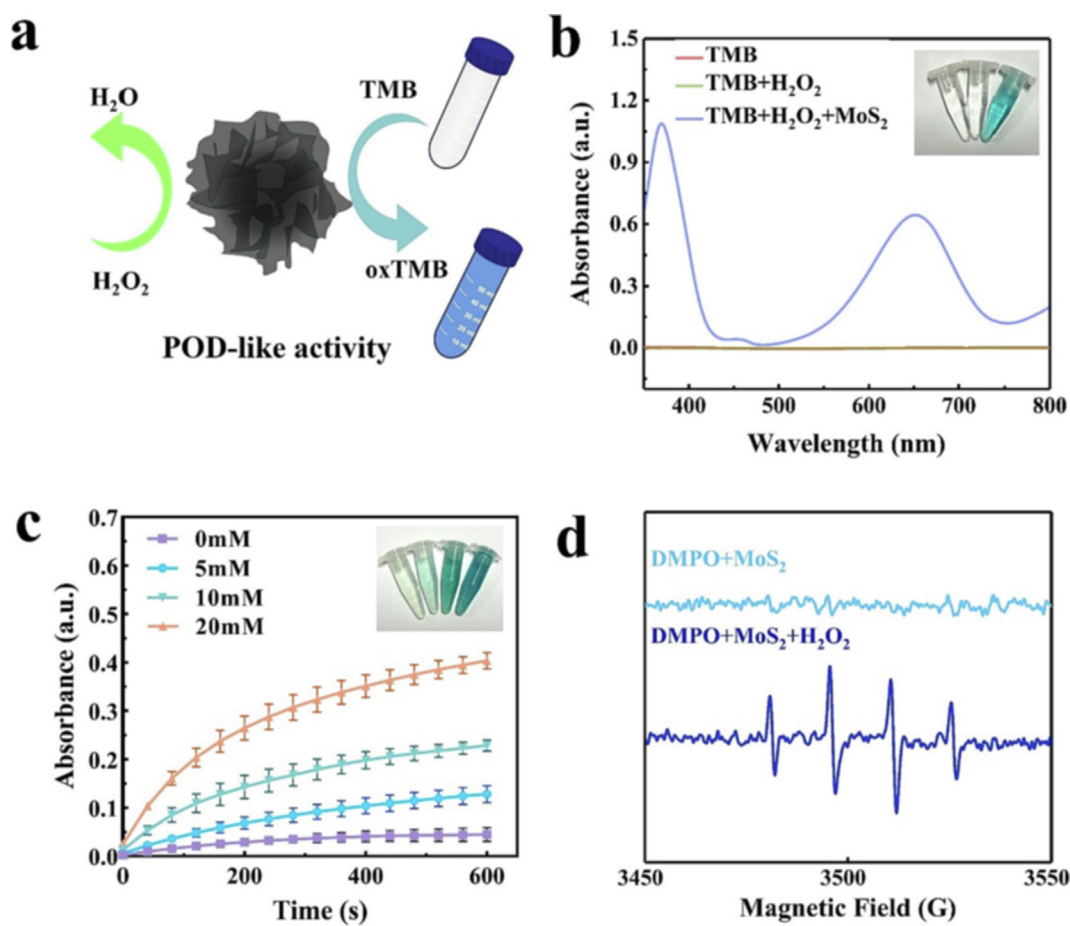


Fig. 4 (a) Schematic diagram of MoS₂ POD-like activity, (b) Ultraviolet visible absorption spectra of different groups of oxTMB and corresponding color developing solution (in order from left to right: TMB, TMB + H₂O₂, TMB + H₂O₂ + MoS₂), (c) Time dependent absorbance of oxTMB after treatment with different H₂O₂ concentrations (0, 5, 10, and 20 mM) and the corresponding color development solutions (in order from left to right: 0, 5, 10, and 20 mM), (d) Spin-trapping ESR spectra of DMPO in MoS₂ under different conditions.

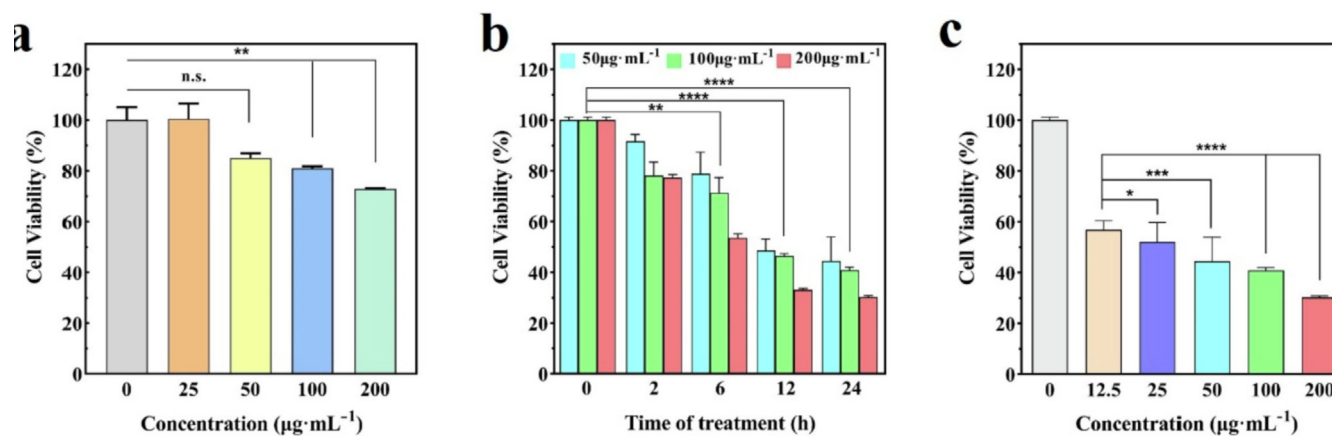


Fig. 5 (a) Cell viability of L929 was incubated with MoS₂ at 0–200 µg/ml concentration gradient for 24 h, (b) The cell viability of 4 T1 was incubated at different concentrations of MoS₂ at 50, 100, and 200 µg/mL concentrations, (c) Cell viability of 4 T1 was incubated with MoS₂ at 0–200 µg/ml concentration gradient for 24 h. (**P* < 0.05, ***P* < 0.01, ****P* < 0.001, *****P* < 0.0001, *n* = 4 independent measurements, values are means ± SEM).

a large amount of apoptosis due to the release of MoS₂ effective therapeutic substances. It was observed that 4 T1 cell wall was broken and a large number of cells were suspended. The

co-staining results of living and dead cells are consistent with the results of CCK-8, indicating that MoS₂ can be used as an effective cancer therapeutic agent.

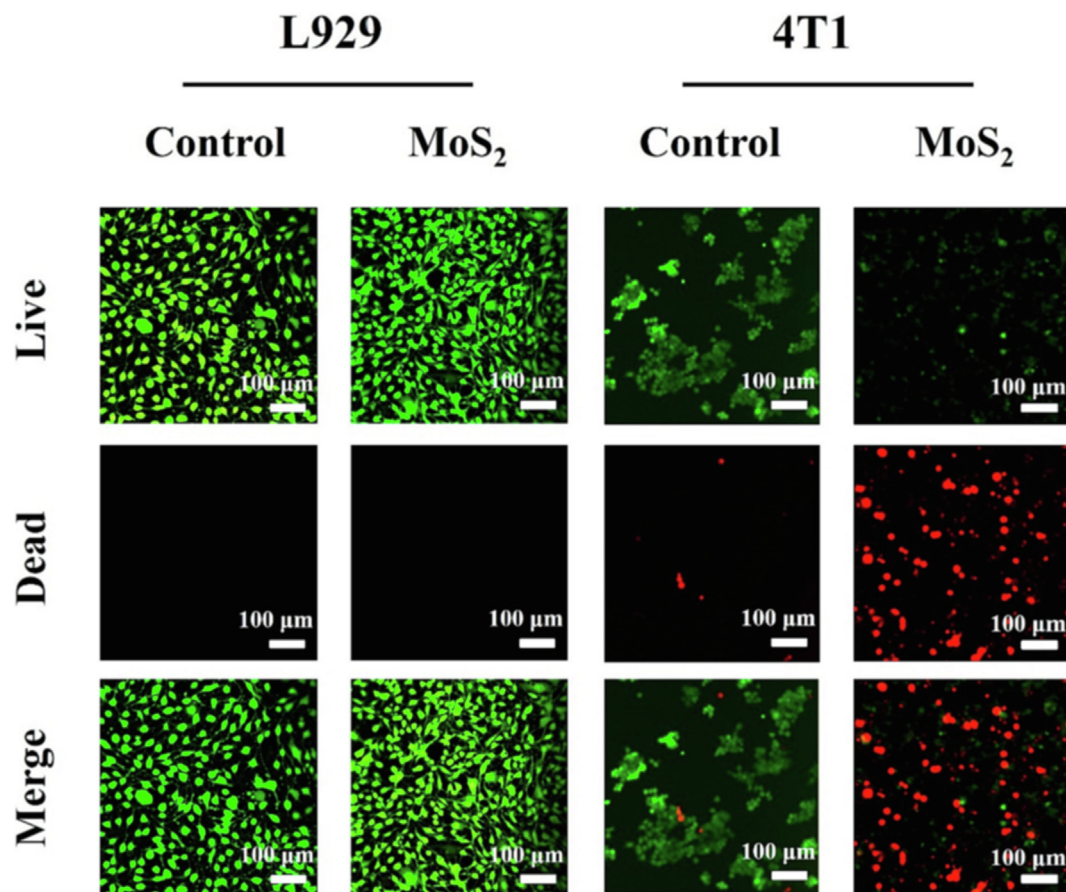


Fig. 6 Laser copolymerization microscope images of AM and PI co-staining L929 and 4 T1.

4. Conclusion

To sum up, MoS₂ has been successfully prepared by the molten salt method at low temperatures in this study. It can show high-efficiency tumor inhibition when acting on 4 T1 alone. MoS₂ has the potential to be an efficient therapeutic nanocarrier with synergistic CDT therapeutic effect. SEM and HRTEM show that the accumulation of popcorn-like spherical structure of MoS₂ has the characteristics of large surface area and a large number of defects in the edge gullies which make it easier to modify the surface function. ESR experiment shows that MoS₂ can stably produce a large amount of -OH. The proliferation experiment *in vitro* shows that 4 T1 produced oxidative stress under the action of MoS₂ and caused significant apoptosis of cancer cells. Compared with the effect of inhibiting tumor cell proliferation, MoS₂ showed little cytotoxicity on L929. Since MoS₂ has peroxidase like activity and can catalyze the generation of ROS oxide rich in the acidic environment of tumors, its uptake by tumor cells is higher. MoS₂ can be used as an effective therapeutic agent to inhibit tumor cells. The high specific therapeutic effect of MoS₂ on tumors shows that it can be used as an effective cocatalyst nanocarrier, and its surface modification as a substrate to further enhance the anticancer effect is our research direction in the future.

Declaration of Competing Interest

The authors declare that they have no known competing financial interests or personal relationships that could have appeared to influence the work reported in this paper.

Acknowledgments

The authors gratefully acknowledge the financial support from National Natural Science Foundation of China (No. 51772209) and the Postgraduate Innovation Research Projects of Tianjin Normal University (No. 2022KYCX024Z).

Disclosure of Competing Interest

The authors declare that they have no known competing financial interests or personal relationships that could have appeared to influence the work reported in this paper.

References

- Abbas, F., Jan, T., Iqbal, J., Ahmad, I., Naqvi, M.S.H., Malik, M., 2015. Facile synthesis of ferromagnetic Ni doped CeO₂ nanoparticles with enhanced anticancer activity. *Appl. Surf. Sci.* 357, 931–936. <https://doi.org/10.1016/j.apsusc.2015.08.229>.
- Arami, H., Khandhar, A., Liggitt, D., Krishnan, K.M., 2015. In vivo delivery, pharmacokinetics, biodistribution and toxicity of iron oxide nanoparticles. *Chem. Soc. Rev.* 44, 8576–8607. <https://doi.org/10.1039/C5CS00541H>.
- Bullo, S., Buskaran, K., Baby, R., Dorniani, D., Fakurazi, S., Hussein, M.Z., 2019. Dual drugs anticancer nanoformulation using graphene oxide-PEG as nanocarrier for protocatechuic acid and chlorogenic acid. *Pharm. Res.* 36, 1–11. <https://doi.org/10.1007/s11095-019-2621-8>.

- Chen, F., Luo, Y., Liu, X., Zheng, Y., Han, Y., Yang, D., Wu, S., 2022. 2D molybdenum sulfide-based materials for photo-excited antibacterial application. *Adv. Healthcare Mater.* 11, 2200360. <https://doi.org/10.1002/adhm.202200360>.
- Chong, C., Liu, H., Wang, S., Yang, K., 2021. First-principles study on the effect of strain on single-layer molybdenum disulfide. *Nanomaterials* 11, 3127. <https://doi.org/10.3390/nano11113127>.
- Curigliano, G., Cardinale, D., Dent, S., Criscitiello, C., Aseyev, O., Lenihan, D., Cipolla, C.M., 2016. Cardiotoxicity of anticancer treatments: Epidemiology, detection, and management. *CA Cancer J. Clin.* 66, 309–325. <https://doi.org/10.3322/caac.21341>.
- Fan, X., Gaddam, R.R., Kumar, N.A., Zhao, X.S., 2017. A hybrid Mg^{2+}/Li^{+} battery based on interlayer-expanded MoS_2 /graphene cathode. *Adv. Energy Mater.* 7, 1700317. <https://doi.org/10.1002/aenm.201700317>.
- Feng, Z., Liu, X., Tan, L., Cui, Z., Yang, X., Li, Z., Zheng, Y., Yeung, K.W.K., Wu, S., 2018. Electrophoretic deposited stable Chitosan@ MoS_2 coating with rapid in situ bacteria-killing ability under dual-light irradiation. *Small* 14, 1704347. <https://doi.org/10.1002/smll.201704347>.
- Gao, S., Zhou, H., Cui, S., Shen, H., 2018. Bottom-up synthesis of MoS_2 nanospheres for photothermal treatment of tumors. *Photochem. Photobiol. Sci.* 17, 1337–1345. <https://doi.org/10.1039/c8pp00198g>.
- Gao, S., Lin, H., Zhang, H., Yao, H., Chen, Y., Shi, J., 2019. Nanocatalytic tumor therapy by biomimetic dual inorganic nanozyme-catalyzed cascade reaction. *Adv. Sci.* 6, 1801733. <https://doi.org/10.1002/advs.201801733>.
- Gao, L., Zhuang, J., Nie, L., Zhang, J., Zhang, Y., Gu, N., Wang, T., Feng, J., Yang, D., Perrett, S., Yan, X., 2007. Intrinsic peroxidase-like activity of ferromagnetic nanoparticles. *Nat. Nanotechnol.* 2, 577–583. <https://doi.org/10.1038/nnano.2007.260>.
- Hanahan, D., Weinberg, R.A., 2011. Hallmarks of Cancer: The Next Generation. *Cell* 144, 646–674. <https://doi.org/10.1016/j.cell.2011.02.013>.
- He, S., Du, H., Wang, K., Liu, Q., Sun, J., Liu, Y., Du, Z., Xie, L., Ai, W., Huang, W., 2020. Low-temperature molten salt synthesis of $MoS_2@CoS_2$ heterostructures for efficient hydrogen evolution reaction. *Chem. Commun.* 56, 5548–5551. <https://doi.org/10.1039/D0CC01726D>.
- Jaya Seema, D., Saifullah, B., Selvanayagam, M., Gothai, S., Hussein, M., Subbiah, S., Mohd Esa, N., Arulselvan, P., 2018. Designing of the anticancer nanocomposite with sustained release properties by using graphene oxide nanocarrier with phenethyl isothiocyanate as anticancer agent. *Pharmaceutics* 10, 109. <https://doi.org/10.3390/pharmaceutics10030109>.
- Jiang, F., Ding, B., Liang, S., Zhao, Y., Cheng, Z., Xing, B., Lin, J., 2021. Intelligent MoS_2 -CuO heterostructures with multiplexed imaging and remarkably enhanced antitumor efficacy via synergetic photothermal therapy/chemodynamic therapy/immunotherapy. *Biomaterials* 268, . <https://doi.org/10.1016/j.biomaterials.2020.120545> 120545.
- Jin, L., Liu, X., Zheng, Y., Li, Z., Zhang, Y., Zhu, S., Jiang, H., Cui, Z., Chu, P.K., Wu, S., 2022. Interface polarization strengthened microwave catalysis of $MoS_2/FeS/Rhein$ for the therapy of bacteria-infected osteomyelitis. *Adv. Funct. Mater.* 32, 2204437. <https://doi.org/10.1002/adfm.202204437>.
- Kasinathan, K., Marimuthu, K., Murugesan, B., Pandiyan, N., Pandi, B., Mahalingam, S., Selvaraj, B., 2021. Cyclodextrin functionalized multi-layered MoS_2 nanosheets and its biocidal activity against pathogenic bacteria and MCF-7 breast cancer cells: Synthesis, characterization and in-vitro biomedical evaluation. *J. Mol. Liq.* 323, . <https://doi.org/10.1016/j.molliq.2020.114631> 114631.
- Kundu, M., Sadhukhan, P., Ghosh, N., Chatterjee, S., Manna, P., Das, J., Sil, P.C., 2019. pH-responsive and targeted delivery of curcumin via phenylboronic acid-functionalized ZnO nanoparticles for breast cancer therapy. *J. Adv. Res.* 18, 161–172. <https://doi.org/10.1016/j.jare.2019.02.036>.
- Li, X., Bi, W., Zhang, L., Tao, S., Chu, W., Zhang, Q., Luo, Y., Wu, C., Xie, Y., 2016a. Single-atom Pt as co-catalyst for enhanced photocatalytic H_2 evolution. *Adv. Mater.* 28, 2427–2431. <https://doi.org/10.1002/adma.201505281>.
- Li, B., Luo, Y., Zheng, Y., Liu, X., Tan, L., Wu, S., 2022. Two-dimensional antibacterial materials. *Prog. Mater. Sci.* 130, . <https://doi.org/10.1016/j.pmatsci.2022.100976> 100976.
- Li, G., Zhang, D., Qiao, Q., Yu, Y., Peterson, D., Zafar, A., Kumar, R., Curtarolo, S., Hunte, F., Shannon, S., Zhu, Y., Yang, W., Cao, L., 2016b. All the catalytic active sites of MoS_2 for hydrogen evolution. *J. Am. Chem. Soc.* 138, 16632–16638. <https://doi.org/10.1021/jacs.6b05940>.
- Liu, J., Cui, L., Losic, D., 2013. Graphene and graphene oxide as new nanocarriers for drug delivery applications. *Acta Biomater.* 9, 9243–9257. <https://doi.org/10.1016/j.actbio.2013.08.016>.
- Liu, J., Huang, H., Ge, C., Wang, Z., Zhou, X., Fang, Y., 2022. Boosting CdS photocatalytic activity for hydrogen evolution in formic acid solution by P doping and MoS_2 photodeposition. *Nanomaterials* 12, 561. <https://doi.org/10.3390/nano12030561>.
- Lv, R., Liang, Y., Li, Z., Zhu, S., Cui, Z., Wu, S., 2022. Flower-like $CuS/graphene$ oxide with photothermal and enhanced photocatalytic effect for rapid bacteria-killing using visible light. *Rare Met.* 41, 639–649. <https://doi.org/10.1007/s12598-021-01759-4>.
- Mousavi, S.M., Hashemi, S.A., Ghasemi, Y., Amani, A.M., Babapoor, A., Arjmand, O., 2019. Applications of graphene oxide in case of nanomedicines and nanocarriers for biomolecules: review study. *Drug Meta. Rev.* 51, 12–41. <https://doi.org/10.1080/03602532.2018.1522328>.
- Mout, R., Moyano, D.F., Rana, S., Rotello, V.M., 2012. Surface functionalization of nanoparticles for nanomedicine. *Chem. Soc. Rev.* 41, 2539–2544. <https://doi.org/10.1039/C2CS15294K>.
- Murugesan, B., Sonamuthu, J., Samayanan, S., Arumugam, S., Mahalingam, S., 2018. Highly biological active antibiofilm, anticancer and osteoblast adhesion efficacy from MWCNT/PPy/Pd nanocomposite. *Appl. Surf. Sci.* 434, 400–411. <https://doi.org/10.1016/j.apsusc.2017.10.142>.
- Park, K.M., Lee, D.W., Sarkar, B., Jung, H., Kim, J., Ko, Y.H., Lee, K.E., Jeon, H., Kim, K., 2010. Reduction-sensitive, robust vesicles with a non-covalently modifiable surface as a multifunctional drug-delivery platform. *Small* 6, 1430–1441. <https://doi.org/10.1002/smll.201000293>.
- Ran, J., Gao, G., Li, F.T., Ma, T.Y., Du, A., Qiao, S.Z., 2017. Ti_3C_2 MXene co-catalyst on metal sulfide photo-absorbers for enhanced visible-light photocatalytic hydrogen production. *Nat. Commun.* 8, 1–10. <https://doi.org/10.1038/ncomms13907>.
- Ranucci, E., Suardi, M.A., Annunziata, R., Ferruti, P., Chiellini, F., Bartoli, C., 2008. Poly (amidoamine) conjugates with disulfide-linked cholesterol pendants self-assembling into redox-sensitive nanoparticles. *Biomacromolecules* 9, 2693–2704. <https://doi.org/10.1021/bm800655s>.
- Saifullah, B., Buskaran, K., Shaikh, R.B., Barahue, F., Fakurazi, S., Mohd Moklas, M.A., Hussein, M.Z., 2018. Graphene oxide-PEG-protocatechuic acid nanocomposite formulation with improved anticancer properties. *Nanomaterials* 8, 820. <https://doi.org/10.3390/nano8100820>.
- Tan, L., Wang, S., Xu, K., Liu, T., Liang, P., Niu, M., Fu, C., Shao, H., Yu, J., Ma, T., Ren, X., Li, H., Dou, J., Ren, J., Meng, X., 2016. Layered MoS_2 hollow spheres for highly-efficient photothermal therapy of rabbit liver orthotopic transplantation tumors. *Small* 12, 2046–2055. <https://doi.org/10.1002/smll.201600191>.
- Wang, L., Huo, M., Chen, Y., Shi, J., 2018. Tumor Microenvironment-Enabled Nanotherapy. *Adv. Healthc. Mater.* 7, 1701156. <https://doi.org/10.1002/adhm.201701156>.
- Wang, C., Li, J., Liu, X., Cui, Z., Chen, D.F., Li, Z., Liang, Y., Zhu, S., Wu, S., 2020. The rapid photoresponsive bacteria-killing of Cu-doped MoS_2 . *Biomater. Sci.* 8, 4216–4224. <https://doi.org/10.1039/D0BM00872A>.

- Wu, S., Liu, X., Ren, J., Qu, X., 2019. Glutathione depletion in a benign manner by MoS₂-based nanoflowers for enhanced hypoxia-irrelevant free-radical-based cancer therapy. *Small* 15, 1904870. <https://doi.org/10.1002/smll.201904870>.
- Wu, J., Zhao, L., Xu, X., Bertrand, N., Choi, W.I., Yameen, B., Shi, J., Shah, V., Mulvale, M., MacLean, J.L., Farokhzad, O.C., 2015. Hydrophobic cysteine poly(disulfide)-based redox-hypersensitive nanoparticle platform for cancer theranostics. *Angew. Chem. Int. Ed.* 54, 9218–9223. <https://doi.org/10.1002/anie.201503863>.
- Xing, M., Xu, W., Dong, C., Bai, Y., Zeng, J., Zhou, Y., Zhang, J., Yin, Y., 2018. Metal sulfides as excellent co-catalysts for H₂O₂ decomposition in advanced oxidation processes. *Chem.* 4, 1359–1372. <https://doi.org/10.1016/j.chempr.2018.03.002>.
- Yang, B., Chen, Y., Shi, J., 2019a. Nanocatalytic medicine. *Adv. Mater.* 31, 1901778. <https://doi.org/10.1002/adma.201901778>.
- Yang, G., Phua, S.Z.F., Bindra, A.K., Zhao, Y., 2019b. Degradability and clearance of inorganic nanoparticles for biomedical applications. *Adv. Mater.* 31, 1805730. <https://doi.org/10.1002/adma.201805730>.
- Yang, Y., Wu, J., Bremner, D.H., Niu, S., Li, Y., Zhang, X., Xie, X., Zhu, L.M., 2020. A multifunctional nanoplatform based on MoS₂-nanosheets for targeted drug delivery and chemo-photothermal therapy. *Colloids Surf. B* 185,. <https://doi.org/10.1016/j.colsurfb.2019.110585> 110585.
- Zhang, J., Bai, T., Huang, H., Yu, M.H., Fan, X., Chang, Z., Bu, X. H., 2020. Metal-organic-framework-based photocatalysts optimized by spatially separated cocatalysts for overall water splitting. *Adv. Mater.* 32, 2004747. <https://doi.org/10.1002/adma.202004747>.
- Zhang, C., Bu, W., Ni, D., Zhang, S., Li, Q., Yao, Z., Zhang, J., Yao, H., Wang, Z., Shi, J., 2016. Synthesis of iron nanometallic glasses and their application in cancer therapy by a localized Fenton reaction. *Angew. Chem.* 55, 2101–2106. <https://doi.org/10.1002/ange.201510031>.
- Zhang, A., Li, A., Zhao, W., Yan, G., Liu, B., Liu, M., Li, M., Huo, B., Liu, J., 2018. An efficient and self-guided chemo-photothermal drug loading system based on copolymer and transferrin decorated MoS₂ nanodots for dually controlled drug release. *Chem. Eng. J.* 342, 120–132. <https://doi.org/10.1016/j.cej.2018.02.081>.
- Zhang, X., Zhao, Z., Yang, P., Liu, W., Fan, J., Zhang, B., Yin, S., 2020a. MoS₂@C nanosphere as near infrared/pH dual response platform for chemical photothermal combination treatment. *Colloids Surf. B* 192,. <https://doi.org/10.1016/j.colsurfb.2020.111054> 111054.
- Zhou, S., Jiao, X., Jiang, Y., Zhao, Y., Xue, P., Liu, Y., Liu, J., 2021. Engineering Eu³⁺-incorporated MoS₂ nanoflowers toward efficient photothermal/photodynamic combination therapy of breast cancer. *App. Surf. Sci.* 552,. <https://doi.org/10.1016/j.apusc.2021.149498> 149498.
- Zhu, M., Liu, X., Tan, L., Cui, Z., Liang, Y., Li, Z., Yeung, K.W.K., Wu, S., 2020. Photo-responsive chitosan/Ag/MoS₂ for rapid bacteria-killing. *J. Hazard. Mater.* 383,. <https://doi.org/10.1016/j.jhazmat.2019.121122> 121122.